Hard X-Ray Microprobe

Antonio Lanzirotti and Steve Sutton
Consortium for Advanced Radiation Sources
The University of Chicago
lanzirotti@bnl.gov

Introduction

Beamline X26A at National Synchrotron Light Source (NSLS) has been used as a synchrotron x-ray microprobe since 1986 and remains to this day the only dedicated hard x-ray microprobe available to users at the NSLS. The beamline is operated by a Participating Research Team (PRT) consisting of three member organizations; The University of Chicago's Consortium for Advanced Radiation Sources (CARS), the University of Georgia's Savannah River Ecology Laboratory (SREL), and Brookhaven National Laboratory's Environmental Sciences Department. Although a wide array of experiments are conducted at the beamline spanning the breadth of scientific disciplines represented by visiting scientists to the NSLS, the core research mission of X26A remains in Earth and Environmental Sciences. Synchrotron-based micro-analytical research has a major impact in advancing our understanding of the speciation, transport, and reactions of chemical species in the Earth. X-ray microprobe techniques offer distinct advantages over other analytical techniques by allowing analyses to be done *in-situ*, an important example being the ability to determine chemical speciation of a wide variety of toxic elements in moist soils and biological specimens with little or no chemical pretreatment and low detection limits. In particular, microXAFS allows one to quantify oxidation state ratios in heterogeneous earth materials and individual mineral grains. Such information is crucial in understanding the toxicity, mobility, and containment of contaminating metals in the environment, mechanisms of trace element partitioning, and paths of strategic metal enrichment in nature.

Principles of Hard X-ray Micro-Spectroscopy

Microbeam SXRF

Beamline X26A began its life as a hard x-ray microprobe with a dedicated emphasis on x-ray fluorescence (XRF) microspectroscopy. The x-ray fluorescence technique has long been a basic research tool in chemical analysis. For our purposes, if we consider a sample irradiated with x-rays, two basic types of interactions can occur, photoionization or scattering. In the former, the incident photon ejects an electron from the atom, an electron hole is created and the atom ionized. In the latter, the photon is redirected by an electron with (Compton) or without (elastic) loss of energy. Once the electron hole is created by photoionization, the excited atomic state decays either by an Auger process (radiation-less) or by fluorescence. In the fluorescence process, the resulting vacancy is filled by an outer shell electron and a characteristic x-ray is emitted whose energy is unique for each transition and thereby is used to identify the emitting atom. Transitions filling vacancies in the innermost shell are called K X-rays, those filling the next shell are L X-rays, etc. The intensity of a given fluorescent x-ray is proportional to the concentration of that element in the sample. Thus, an XRF analysis consists of exciting the specimen with an intense x-ray beam and measuring the energies and intensities of emitted x-rays. Quantification of the elemental content based on the XRF spectrum is relatively straightforward since the physics of photon interactions with matter is well understood.

Conventional XRF is typically performed on homogenized, centimeter-sized samples with a laboratory x-ray tube source. The principal advantage of using synchrotron radiation for XRF analysis is that it allows the spatial resolution of the method to be reduced down to the micrometer level. There are several reasons why this is possible. First, the synchrotron radiation is several orders more intense than x-rays from tube sources. Second, the synchrotron beam is well-collimated, so that the intensity remains high at considerable distances from the source. This means that simple apertures and focusing mirrors can be used to produce small, intense beams. Third, synchrotron radiation is highly linearly polarized which allows background from scattered radiation to be minimized by the geometry of the experiment.

Synchrotron XRF (SXRF) is complementary to other microanalysis techniques, such as electron microprobe (EMP) analysis, particle induced x-ray emission (PIXE), laser ablation inductively coupled plasma mass spec-

trometry (LA-ICP-MS) and secondary ion mass spectrometry (SIMS). Each of these techniques is optimized for particular applications, elements, or sample types. The attractiveness of SXRF lies in its capability for non-destructive, trace level analyses of a wide range of elements with high spatial resolution. Another advantage is the low power deposition, a particularly important consideration when analyzing volatile-rich specimens or biological materials. For a given fluorescent signal, X-rays deposit between 10^{-3} and 10^{-5} times less energy than charged particles.

The SXRF microprobe is particularly well suited for (1) trace element analysis of nanogram samples (e.g., various types of particles, aerosols, and inclusions) and (2) characterization of trace element distributions with high spatial resolution (e.g., diffusion profiles, chemical zonation, impurity distribution, and compositional mapping).

Microbeam XANES

Although the principal focus of the X26A microprobe remains XRF analysis, microbeam X-ray absorption fine-structure spectroscopy (XAFS) has become a routine analytical tool available to the X26A user. XAFS can be used as a local structural probe, usually of the first two shells of atoms around an absorber atom, potentially providing information on valance state, average interatomic distances, and the number and chemical identities of nearest neighbors. For simplicity, X-ray absorption spectra are typically divided into two energy regions. The region extending from a few eV below an element's absorption edge to about 50 eV above is generally referred to as the X-ray Absorption Near-Edge Structure of the spectrum or XANES region. The most common information available from XANES spectra is the valence state of the absorber. Under ideal conditions XANES spectra can also yield information about the coordination number of the absorber.

The Extended X-ray Absorption Fine Structure or EXAFS region extends to higher energy, typically up to about 1000 eV above the edge. Electron scattering in the vicinity of the absorber produces EXAFS spectra. Detailed evaluation of the oscillations in the spectra can yield information about coordination numbers and bond lengths.

However, most X26A users doing XAFS analysis focus on the XANES region. Very reliable XANES data can typically be obtained even for low abundance trace elements. X26A can be used to yield very good EXAFS data at low concentration on big, homogenized samples, particularly when utilizing larger diameter beams. Obtaining high-resolution microEXAFS data is more of a challenge. Very little work has been published pertaining to the experimental difficulties of conducting micro-EXAFS. Most micro-spectroscopy is measured in fluorescence and as spot size and sample thickness moves below 1 μm, difficulties of self-absorption become less important. However, if the sample size is greater than about 10 μm in thickness, then self-absorption effects within the volume excited by the incident X-rays can become an issue. This is less of an issue with XANES measurements, but micro-EXAFS measurements offer unique challenges. If the sampling area is of the same size as the probe beam, then small deviations in beam position on the sample can dramatically effect the EXAFS measurements. The primary reason for this is that the EXAFS signal is typically less than 1% of the total signal. For a 10-μm sized beam a relative drift on the order of 0.1 μm can be significant in some cases. Such dimensions are on the order of thermal expansion/contraction of the sample holder with subtle temperature variations. So for microbeam EXAFS at X26A it's wisest to ensure that the measured area is homogeneous on a scale larger than the probe beam and that sample stage stability is given consideration. Obviously in the real world this isn't always possible, but with the SXRF capabilities of the beamline a user can produce an elemental map of the selected sample areas to ensure that sample spatial homogeneity is larger than the spot size of the probe beam. Sample thickness can similarly affect XAFS measurements, particularly in transmission mode.

At X26A, however, most XAFS analysis is conducted in fluorescence mode, which is typically better suited to the types samples used at X26A. For most users, samples have potentially variable thickness, are often compositionally heterogeneous on a micron scale, and are typically mounted on glass slides. Additionally, the majority of users are most interested in XAFS of trace elements, rather than major elements, which is also better suited to fluorescence mode analysis.

Microbeam XRD

Over the past three years X26A has embarked on a feasibility study in micro-crystallography, combining the microbeam XRF and XAFS capabilities of the beamline with the unique mineralogic information potentially provided by microbeam X-ray diffraction (XRD). The small beam divergence and high brightness the synchrotron source provides has significant potential in the development of microbeam XRD for earth sciences. For geologic and environmental samples where grain sizes are typically in the μm range and fine-scale mineralogic heterogeneity is expected, combined microbeam XRD-XRF-

XANES provides a unique method by which crystallographic, compositional, and redox state data can be gathered near simultaneously. For environmental studies in particular, where contaminants are typically adsorbed onto mineral surfaces and extraction of these contaminants is virtually impossible, microbeam XRD has significant potential in allowing the user to quantify the mineralogy of these contaminant phases *in-situ* and map their variability over millimeter or micron scales. Coupling the XRD analysis with microbeam XRF analysis means that analyses can be confidently restricted to areas where contaminants are localized. Coupling XRD with XAFS gives a means of validating the speciation, coordination geometry, and bond lengths calculated by XANES and EXAFS.

At X26A our diffraction studies focus primarily on *in-situ* phase identification using standard powder methods. As such, some natural limitations exist that must be kept in mind. Given that most earth materials tend to be mounted on glass slides for analysis, such backing materials produce low angle scatter that can interfere with the identification of minerals. Free standing, epoxy mounts work best for these types of analyses, but may not always be feasible. Also, since most of these analyses are more conveniently done in transmission mode geometry (primarily due to space limitations on the experimental table) sample thickness and density should be low enough to permit the diffracted x-rays to penetrate and for analysis points to be representative (sample thickness < 100 μm seem to work best). Lastly, due to the small diameter of the incident beam (typically ~10 μm in diameter), in some samples the crystallites may not be small enough to produce well-defined Debye-Scherrer rings. Rotating the sample during analysis can be used to achieve a more statistically averaged pattern. Future installation of dedicated Phi and Chi rotational stages will allow this to be done more conveniently and expand the capabilities for doing single crystal XRD analysis.

On the other hand, differences in the "spottiness" of the powder pattern can yield important information about the differences in the crystallinity of mineral phases in the sample or preferred grain orientation (**Figure 1**).

During this feasibility study John Parise at SUNY Stony Brook supplied the beamline with a Bruker SMART 1000 CCD system for this purpose. During this study we were able to demonstrate that such a system installed at X26A was capable of producing high-resolution powder diffraction data on very small (<10 μm) crystals *in-situ* within geologic materials while allowing simultaneous x-ray fluorescence and absorption analysis. We expect a dedicated SMART 1500 CCD system to be installed at the beamline in the fall of 2002.

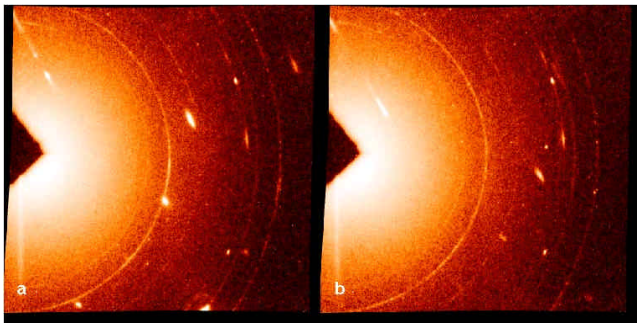

Figure 1*. Two microbeam XRD spectra from a ~10 μm diameter interplanetary dust particle (Flynn et al., 2000). The particle is mostly coarsely crystalline pyrrhotite, which yields the brightly diffracting single points. Upon atmospheric heating, however, finely crystalline magnetite is formed on the pyrrhotite surface, which gives well-defined Debye-Scherrer rings.*

X26A Beamline Configuration

Beamline X26A can be operated with various types of incident synchrotron beams including:

- collimated white beam
- collimated monochromatic beam
- focused white beam
- focused monochromatic beam

By far, the majority of the research conducted at the beamline within the past few years has used focused monochromatic radiation. Prior to the installation of Kirckpatrick-Baez (KB) micro-focusing mirrors, most analyses were done using collimated white beam. The following sections describe the various components of the X26A beamline and associated microprobe apparatus.

Beamline Geometry, Vacuum, and Helium Systems

The synchrotron radiation source is a dipole bending magnet in the electron storage ring. A mask close to the ring delivers 5 mRad of radiation down the beamline to the experimental hutch 9 meters from the source. The maximum flux delivered to sample at 10 μm size is energy dependent, but for X26A is typically 10^8 to 10^9 ph/s/0.01%BW. Starting at the storage ring end of the beamline the basic components are (**Figure 2**):

- Water-cooled beryllium window to isolate the beamline vacuum from the ring vacuum.
- First beamline aperture consisting of a fixed width, horizontal slit and a vertical, V-slit which can be moved independently to produce a beam about 1 mm in size. Both slits are water-cooled.
- A monochromator tank that contains two silicon channel-cut monochromator crystals

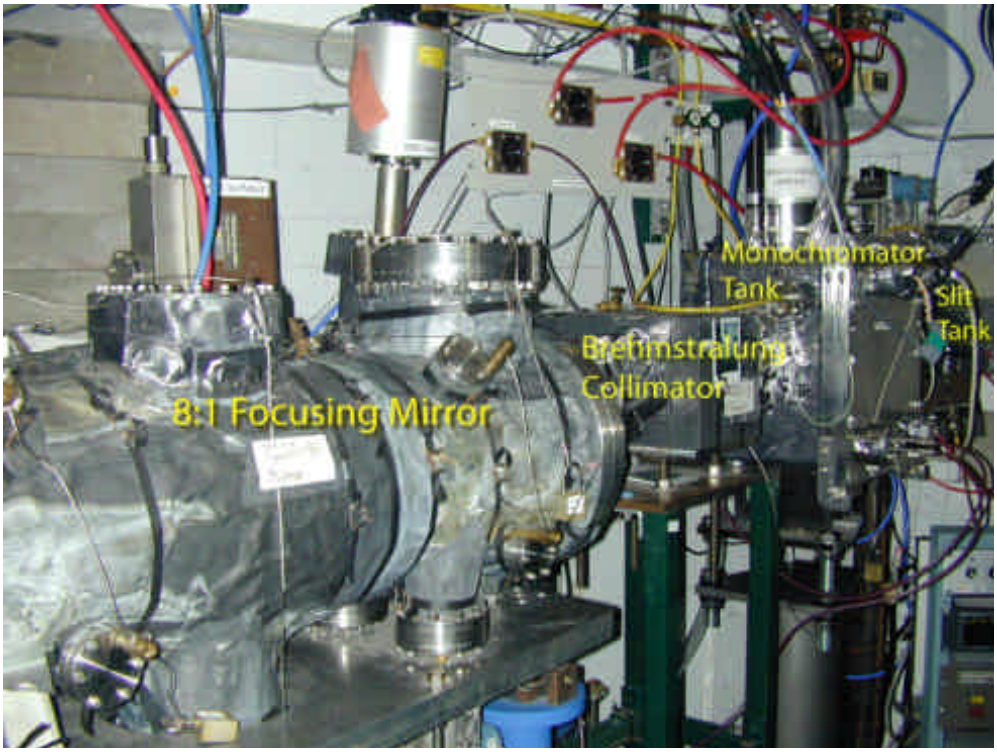

***Figure 2**. X26A beamline components.*

(Si(111) and Si(311)) for selecting x-rays of a given energy from the white synchrotron spectrum. These crystals are water cooled (~10°C) and reside in a helium environment. The housing has a Be window on each end. This device can be either in or out of the beam.

- 8:l ellipsoidal focusing mirror for focusing either the direct white beam or the monochromatic beam. The mirror tank has a Be window on the downstream end and operates in vacuum. This device can be either in or out of the beam. With the installation of the KB mirror system, this focusing mirror is typically not used because it can only focus down to about 200 μm.
- Four-jaw motor-driven Ta-slit assembly for continuous adjustment of beam size from several centimeters down to several tens of micrometers. This is typically set to 350 μm as an entrance slit for the KB mirrors.
- Ion chamber with helium for monitoring the beam intensity transmitted by the four-jaw slits.
- Experimental hutch containing the microprobe apparatus and interlocked for personnel safety.

Most of the beamline is under high vacuum ranging between 10^{-8} to 10^{-9} torr maintained with ion pumps. The exceptions are the monochromator housing that is kept under helium to improve crystal cooling and the four-jaw/ion chamber housing where helium ionization is used for the intensity measurement. Three of the Be windows act as barriers between the helium and high vacuum segments. Low energy photons (< 3 keV) are absorbed primarily in the first Be window which is constantly water cooled.

Monochromator

The X26A monochromator (**Figure 3**) uses two silicon channel-cut crystals to "tune" and scan the energy of the x-ray beam allowed to enter the experimental hutch. The two monochromator crystals are monolithic crystals that have had a channel bored down their centers to expose two parallel surfaces. The white beam impinges on the first crystal face (oriented at some non-zero angle) and X-rays with the wavelength λ that satisfy the Bragg equation ($n\lambda = 2d\sin\theta$; n an integer, d the planar spacing and θ the reflection angle) are reflected. This monochromatized beam strikes the second crystal face, which reflects it along a horizontal but offset trajectory. The X26A design is unique in that it incorporates two, side-by-side, channel-cut crystals, each crystal with a different lattice cut, one a Si(111) and the other a Si(311). The two crystals cover a different, but overlapping, energy range from 4 to 50 keV. The two crystals sit on a translator that allows remote, on-demand translation between the two crystals where the translation is perpendicular to the x-ray beam direction. The crystal holder/translation assembly is mounted to a Huber 410 with 20:1 gear reducer that provides angular control (0.05 eV at 7 keV with Si(111)). The crys-

tals are separated laterally by 6 mm to allow white beam to travel between them even at non-zero rotation stage positions (thereby allowing rapid changes between monochromatic and white beam operations). For experiments requiring large horizontal white beam fans (e.g., microtomography), the tank height can be adjusted to allow direct beam to travel above the crystals when the crystals are at zero degrees. Both crystals have vertical offsets of about 14 mm above the position of the direct white beam. The monochromator can be used both for selective excitation in trace element microanalysis and for XAFS.

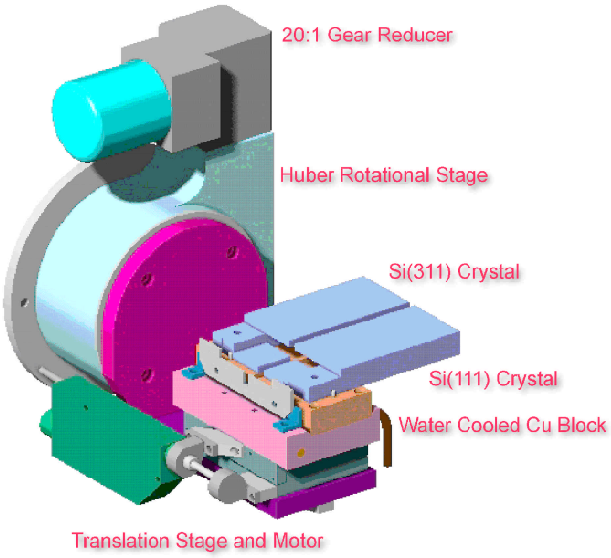

***Figure 3**: X26A dual crystal monochromator assembly.*

Beam Collimators

Although in principle there are many ways to produce x-ray microbeams, at X26A we've basically used collimation and focusing. It is relatively easy to collimate the beam. The only limitation is that the flux of the photons through the hole should remain high enough to give good sensitivity in a reasonable time. However, higher fluxes can be obtained with focusing optics and on X26A virtually all monochromatic studies make use of our system of Kirkpatrick-Baez microfocusing mirrors (**Figure 4**). Upstream of these mirrors two beam collimation systems are used to reduce beam size in manageable increments. The first collimator, called the aperture, consists of a fixed width, horizontal slit and a vertical, V-slit which can be moved independently to produce a beam about I mm in size. The second collimation system, a tantalum four-jaw slit assembly, can then reduce this beam, either as white or monochromatic radiation, down further. In white beam mode we typically collimate this beam to roughly 30 μm in size using the four-jaws and then use a pinhole collimator immediately upstream of the sample within the hutch to produce a beam size of about 8 μm. With the KB mirror system we typically collimate the monochromatic beam to 350 μm in width (the widest usable beam that will not overfill the mirrors). This 350 μm can then be focused to about 10 μm in diameter.

Focusing Optics

Focusing optics for X-rays remain a great challenge. Potentially useful devices include Fresnel zone plates, Kirkpatrick-Baez multilayer mirrors, tapered glass capillaries, refractive lenses, and critical reflection, focusing mirrors. In the past X26A has used an aluminum, ellipsoidal focusing mirror which produces a focused beam in the hutch about l/8 the size of the source, i.e., about 200 μm. Although still available, this system is

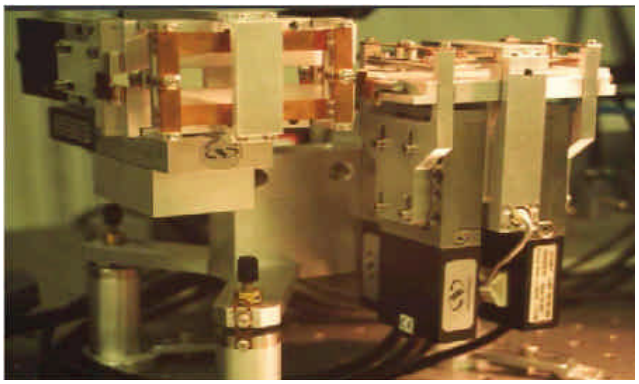

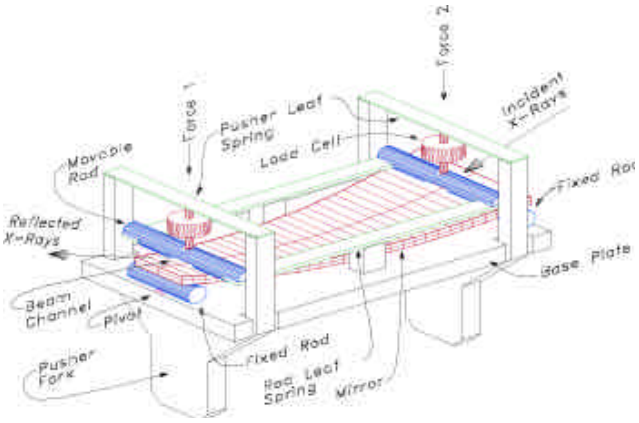

***Figure 4**: Trapezoidal mirror bender showing the two bending forces applied to the movable rods through a load cell attached to a leaf spring to achieve an ellipsoidal surface. The pusher forks are attached to precision translation stages (not shown). A downward motion of the fork increases the load on the mirror. Two such assemblies are arranged in a Kirkpatrick-Baez geometry (one horizontal and one vertical) to achieve spot focusing. (From Eng et al. 1995).*

seldom used. It was found that even with focusing it was still necessary to use a pinhole collimator in order to produce microbeams with this system, and thus limiting the available beam flux. Additionally, the device has a high-energy cutoff at about 14 keV which precludes excitation of any absorption edges above that energy.

In 1997 the X26A PRT installed a set of microfocusing Kirkpatrick-Baez mirrors, which has had a major impact on analytical capabilities particularly in terms of microbeam applications of XAFS spectroscopy. In 1999 these were further upgraded to a new system designed by Peter Eng (CARS) with a smaller footprint and improved focusing. Two separate mirrors focus the beam horizontally and vertically. The mirrors are dynamically bent to elliptical shapes using a mechanical bender. The mirrors themselves are Rh-coated silica. Flux loss due to the reflectivity of the mirrors is roughly 20%. These mirrors (9 meters from the source) focus a 350 x 350 μm monochromatic beam down to 10 (vertical) x 14 (horizontal) μm (FWHM) resulting in a gain (flux/mm^2) of about 1000 over a pinhole. The Kirkpatrick-Baez optics have the advantage of large working distances (50 mm from the downstream end of the second mirror), achromatic operation, i.e. no refocusing is required as the monochromator energy is scanned, and fixed offset. This has enhanced sensitivity significantly for microspectroscopy.

Microprobe Apparatus

Once focused the beam travels through air to the sample mounted vertically at 45° to the incident beam (**Figure 5**). A horizontally mounted Nikon Optiphot petrographic microscope with TV attachment views the sample normal to its surface. Typically, a 5x or 20x (long working distance) objective is used giving about 2 or 0.5 mm fields of view, respectively, on the TV monitor outside the hutch. Transmitted or reflected illumination is available. The entire microprobe apparatus, including mirrors, sample stage, optical microscope, and x-ray detector, rests on a 1 x 0.6 m breadboard that in turn sits on a motor-driven lift table. The lift table allows the entire instrument to be positioned at the correct vertical height to intercept the most intense and most highly polarized portion of the synchrotron radiation profile. Several types of x-ray detectors are in use:

- A Canberra SL30165 Si(Li) detector (resolu tion about 150 eV at Mn Ka).
- A MicroSpec WDX-3 curved-crystal, wavelength dispersive spectrometer (WDS) with 4 analyzer crystals for high energy resolution detection in the 3 to 17 keV range.

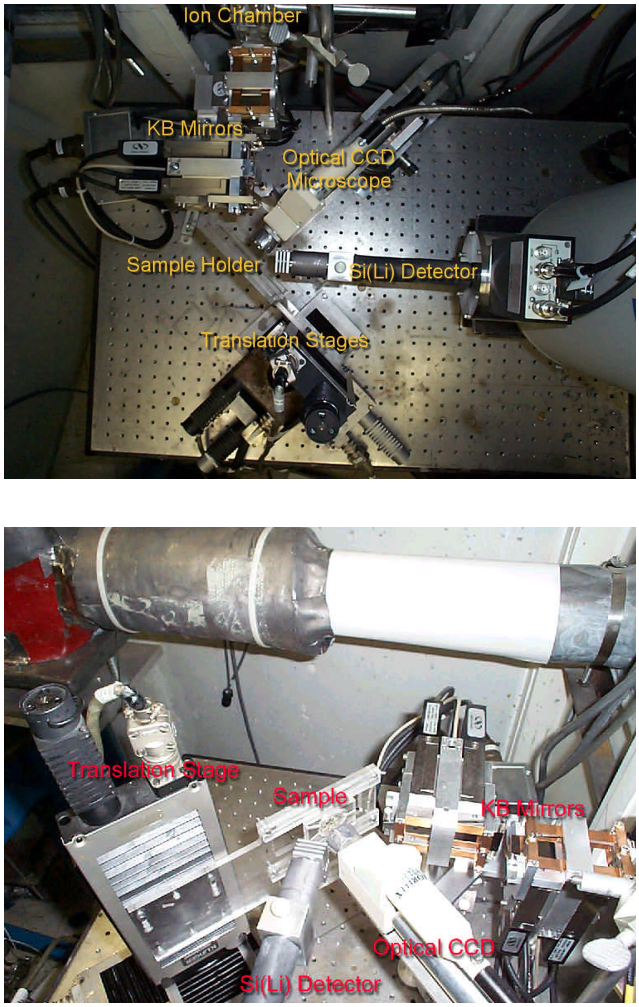

***Figure 5**: Two images of the X26A experimental table.*

- A Canberra 790-7S 9-element LEGe hard x-ray advanced array detector. The system employs digital signal processing using XIA's DXP digital spectrometers (expected delivery, summer 2002).
- Bruker SMART 1500 CCD diffractometer, opti mized for collection of data out to high 2 theta angles and on very weakly diffracting samples (expected delivery fall 2002).
- Custom made mini ion-chambers and pin diode detectors for transmission x-ray detection.

Each of these detectors is optimum for particular types of experiments. For most experiments fluorescence and scattered x-rays from the sample are detected using our Si(Li) energy dispersive detector mounted at 90 degrees to the incident beam and within the storage ring plane (photon polarization plane). The 9-element array detector is optimal for high-count rate work such as microbeam XAFS. The WDS is optimal when improved peak resolution is needed, such as when looking at REE L fluorescence lines where peak overlaps

are severe. Unfortunately this detector requires high flux and is thus typically best used in white beam mode. The CCD diffractometer can be used simultaneously with our Si(Li) and Ge-array solid state detectors for XRD analysis. Our mini ion-chamber and pin diode detectors are used for either flux monitoring or transmission mode XAFS analysis.

Detection Limits

In practice, XRF analyses of trace elements are restricted to the energy interval 3-30 keV. The sensitivity is poor at low energy because of absorption by the Be windows and air paths, and low photoionization cross sections. At high energy, the production of synchrotron radiation decreases by about 1 order of magnitude for every 10 keV. Thus, K lines from elements with atomic number between S and Cs are efficiently detected whereas heavier elements require detection of L lines. Detection limits for L lines are somewhat higher than those for K lines of the same energy because the fluorescence yields are smaller. Since the energy resolution of the Si(Li) detector is about 150-250 eV, L lines are often difficult to resolve at low energy (< 7 keV) where overlap with major element K lines is significant. The sensitivity of the XRF measurement is controlled principally by the intensity of the spectral background. Synchrotron radiation from a NSLS bending magnet is about 99.7 % polarized in the horizontal and 0.3 % in the vertical. Scattering of the vertically polarized photons is the major source of background in the XRF spectra. Incomplete charge collection in the detector is a second source of background. While little can be done to diminish the detector background, scattering background is minimal when the detector is positioned at 90° to the incident photon beam and within the storage ring plane.

Detection limits (ppm) are traditionally determined from a measurement on a standard and defined as C * 3 * (wB)/P, where C is the concentration of the element in the standard, P is the net counts in the fluorescence peak and B is the background counts under the 2σ width of the peak. Detection limits typically vary between 0.1 to 10 ppm dependent on the element and the matrix analyzed.

Running the Microprobe Software

In 2000 the PRT installed a new computer control system that replaced the aging VAX workstations at X26A. This new system is PC-based, running Microsoft Windows NT4, and integrates our existing CAMAC electronics (CAMAC Crate, E500 controllers, Real Time Clock, etc.) through a VME crate running EPICS. The drivers and hardware integration were developed by Mark Rivers and is similar to software that is being used by the CARS beam lines at the APS. Not only does the new system bring commonality between the CARS operations at APS and the NSLS, but it provides a convenient upgrade path for beam lines such as X26A that have a pre-existing (and difficult to replace) investment in CAMAC based electronics. The new EPICS based software provides a new level of flexibility on controlling motors and detectors that was not possible in the past (**Figure 6**).

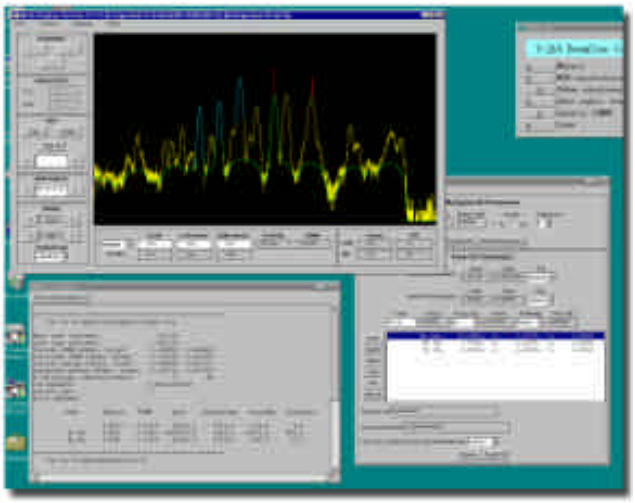

***Figure 6**. Some of the EPICS and IDL control screens. The MCA analyzer window is shown in the upper left.*

It's not feasible here to fully describe the operating software for the beamline. Those interested in examining the operating manuals are directed to our web-site, where we have made these available to users online: http://www.bnl.gov/x26a

But basically the operating system is divided into two sets of beamline controls. MEDM (Motif Editor and Display Manager) is a graphical front-end to EPICS (Experimental Physics Industrial Control System) that we use to physically control beamline motors and electronics through EPICS. MEDM is an extension of EPICS and is a graphical user interface (GUI) for designing and implementing control screens consisting of a collection of graphical objects that display and/or change the values of EPICS process variables. We then simultaneously use IDL (Interactive Data Language) to interact with MEDM in setting up scans, operating the multi-channel analyzer, and process data. Typically both packages need to be running to collect data but only MEDM is needed to move motors, turn on and off MCA, AIM, or HV electronics, etc.

With IDL all scans, data acquisition, and data processing can also be done using GUI's (called widgets in IDL). All these routines are written by us in house and freely distributed to users, who only need to acquire a copy of IDL to use them. IDL is ideally suited to analysis of large matrix arrays (of which we generate many) and its simplicity and modularity in programming allows us to rapidly modify programs as our needs change.

Making a Measurement

The main steps in making an XRF measurement are:

- Sample preparation
- Instrument alignment including establishing the precise location of the beam
- Detector calibration
- Filters selection
- Pulse processing electronics setup
- Detector count rate optimization
- Counting time estimation
- Spectrum acquisition

Geological specimens are typically prepared either as conventional thin sections (preferably 1" circles) or as individually mounted fragments on thin plastic film. No electrically conducting coating is required. There are 4 main considerations in sample preparation. First, since SXRF is a trace element technique samples must be prepared in a clean manner with clean materials. Avoid touching the sample surface, clean samples prior to analysis and use clean mounting adhesives. Most thermal cements we've found are quite dirty with respect to their trace element content. Epoxies that we have found to be acceptable include Buehler Araldite epoxy, Scotchcast electrical resin, acrylic resins such as LR White, Duco 5 minute epoxy, and cyanoacetate (SuperGlue).

Additionally, the incident x-ray beam commonly penetrates the sample and backing material. The sampling depth for fluorescent x-rays is both matrix and element dependent. As a rule of thumb, highest sensitivity for a particular element will be obtained if the sample thickness is about equal to the 1/e absorption depth for the associated x-ray in the matrix of interest. However, lesser thicknesses at the expense of sensitivity are almost always required so that inclusion-free volumes can be analyzed. For geologic samples with densities on the order of 2.5 g/cm^3, it can be expected that high energy fluorescent x-rays generated from the sample can escape from depths exceeding 300 μm. It is therefore essential that backing materials also be pure. This usually means using pure silica glass slides for thin sections (e.g., Suprasil #2 slides from Heraus Amersil seem to have the lowest trace element contents) or Kapton plastic film for particles. Typical window glass used for most petrographic applications can be notoriously contaminated with Fe, Cu, Zn, and/or As. Scotch tape is also an acceptable mounting material and is generally trace element clean with the exception of Br in the adhesive. One note here, however, is that silicon found in the adhesives of Scotch or Kapton tape can effectively absorb a fair amount of low energy x-rays below 6 keV. If this is a concern it's best to try and keep the front surface of the sample free of these types of materials. Lastly, much of the scattered background radiation observed is from scattering off the sample and its backing material, so it's best to try and keep the thickness of the backing to a minimum. Free standing, parallel surfaced slabs are ideal but usually impractical.

Optical photodocumentation of samples is a real plus when working on the microprobe and since the microprobe uses a petrographic microscope, the photographs will accurately represent the view seen on the TV monitor. If possible, determine major element chemistry and sample thicknesses prior to an experimental session.

Once you're ready to start analyzing it's then necessary to align the microprobe. First, the mirrors or pinhole, microscope, sample stage, and detector must be positioned so that the microscope is looking at the point in space where the incident beam is hitting the sample. The detector sits at 90° to the beam and the microscope at 45°. Since we're using a channel-cut monochromator, as we significantly shift energies between experiments the height of the monochromatic beam changes as well. We can move the four-jaws vertically to reposition on the most intense portion of the beam and then change the height of the entire aligned assembly via the lift table. A zinc sulfide phosphor is used to find the x-ray beam position since it optically fluoresces. This fluorescent beam is then focused to the microscope and its position noted physically on the TV monitor. This defines a single point in space that is the intersection of the microbeam and the focal plane of the microscope. Since our microscope objective has a very short focal length, as long as the sample is optically focused on the monitor you have high confidence of the horizontal beam position.

The detector is usually calibrated using either a variable energy radioactive source, a spectrum of an anorthite glass standard (AN100, Geophysical Lab), or NIST XRF thin film standards. Filters may be required on the detector to suppress intense K fluorescence from major elements, in geologic materials this is principally from Ca and Fe. Typically, Kapton (0.5 mm) is used for the

former and aluminum (0.17 mm) for the latter but the optimum filtering conditions depend very much on the major element concentrations and the goals of a particular experiment.

The detector's amplifier electronics can be set for shaping times ranging from 0.5 to 12 μsec. A measurement that is sensitivity-limited could use short shaping times so that the maximum count rate can be obtained. On the other hand, a measurement suffering from peak overlap should use higher shaping times for the highest resolution.

As with any solid-state detector, dead time is also an issue. A counting dead time of about 30-40 % is typically optimal, yielding the highest count rate in terms of counts per clock time. But in order to ensure that the counts/pixel in fluorescent mode are comparable between points that may have different dead time, data is typically collected in 'live time' or detector time. So if you're analyzing a point with 30% dead time, the detector will count 30% longer to account for the difference. Using constant live counting times allows spectra with different dead times to be directly compared. Counting times are determined by the minimum detection limit (MDL) and precision that one is trying to achieve. Both of these parameters can be obtained from a measurement of a suitable standard. Remember, though, that the MDL is a square root function of the counting time so that doubling the counting time leads to a sensitivity improvement of only 40%.

In some cases, however, lower count rates may be necessary. This is particularly true when pileup peaks (spectral artifact caused by two x-rays being sampled simultaneously) interfere with a fluorescence peak of interest. Pile-up peaks can be reduced with a thicker detector filter, by moving the detector further away from the sample, or by adjusting the shaping time of the detector.

The ultimate result of all this is typically an XRF spectrum, a plot of counts as a function of energy usually dividing into 2048 (2K) channels. An example of a "raw spectrum" is shown in **Figure 7**. XRF spectra typically consist of a large number of fluorescence peaks but also artifact peaks such as pileups, escapes and occasionally diffraction peaks. Escape peaks occur when an x-ray excites a Si atom in the detector and the resulting Si Kα fluorescent x-ray (1.74 keV) manages to escape the crystal. Thus, small escape peaks are observed at 1.74 keV below intense peaks in the spectrum. Diffraction peaks are observed from well-ordered samples. If the samples are excited

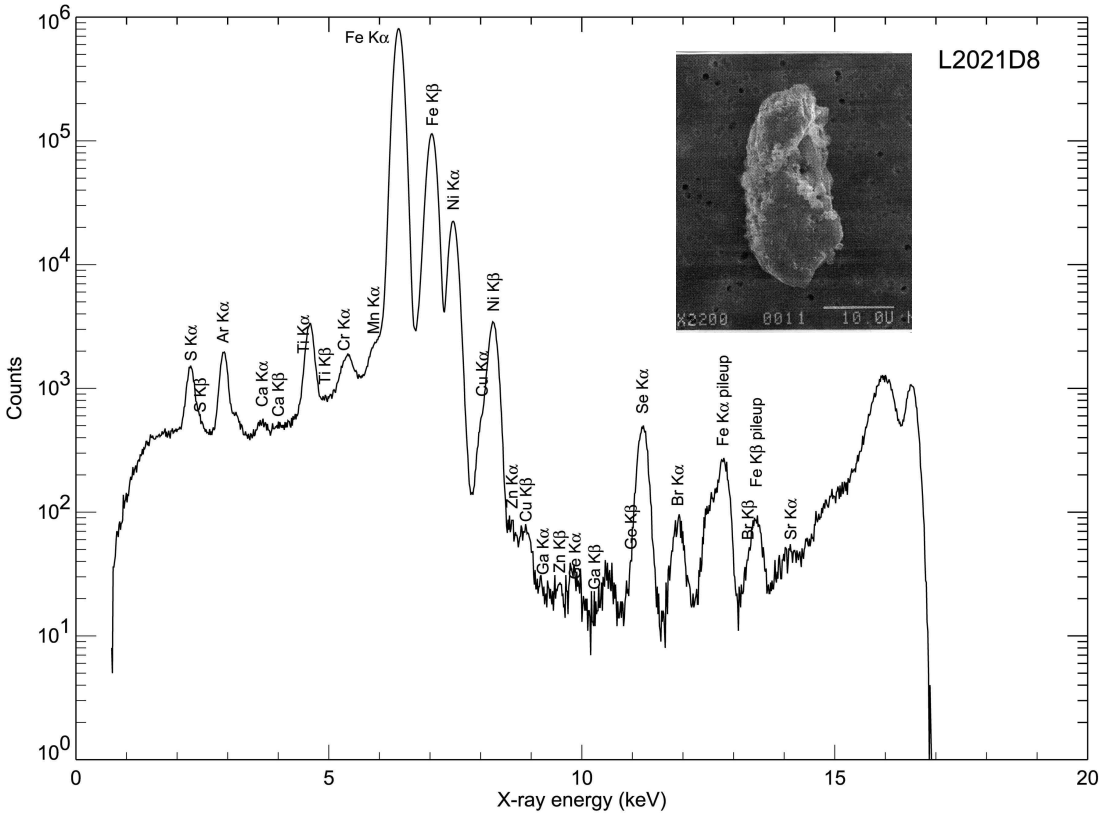

Figure 7. *Energy dispersive XRF spectra of an interplanetary dust particle (Flynn et al., 2000).*

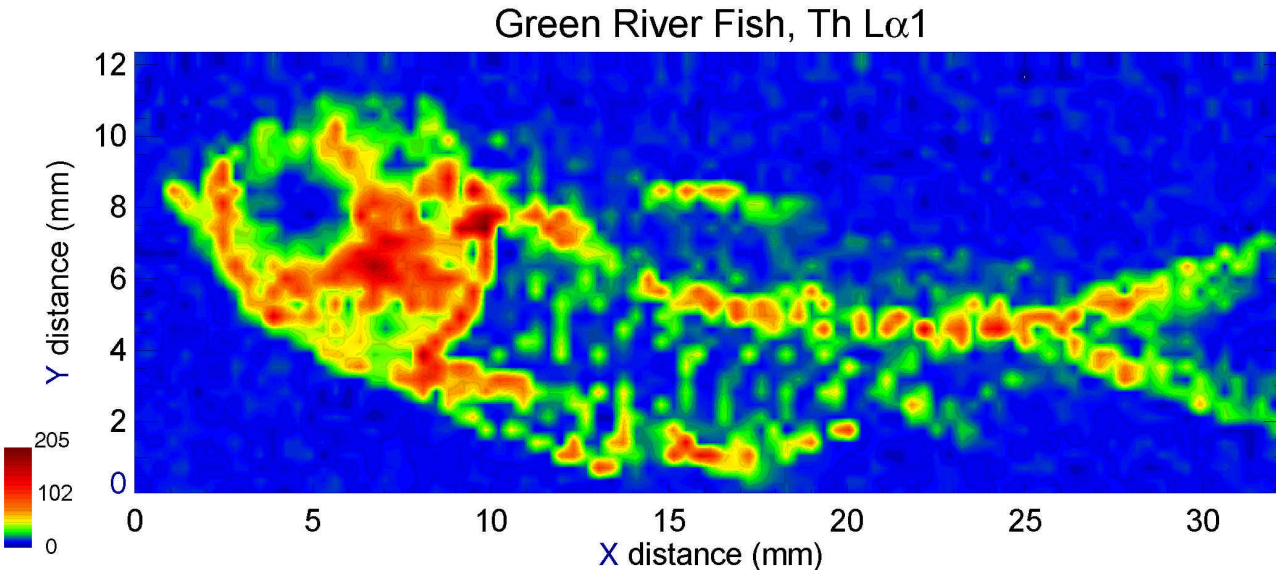

Figure 8. Typical x-ray energy dispersive compositionmal map, this for Th Lα1 fluorescence from a fossilized Cretaceous fish of the Green River Fm. (Cole et al., 2002)

with white light and the energy dispersive detection method is used, lattice planes oriented at 45° to the incident beam can diffract x-rays that satisfy Bragg's Law into the detector and a peak is produced in the spectrum whose energy depends on the lattice plane spacing. Such peaks are identifiable because they (1) occur at energies corresponding to no fluorescence transition, (2) lack companion peaks associated with the fluorescence process and/or (3) change energy and intensity on reorientation of the specimen. Luckily, when using monochromatic radiation such peaks are rarely observed.

During compositional mapping (**Figure 8**) or XAFS analysis, however, we typically don't save the entire XRF spectrum for each pixel. Although we do have the capability of doing this in an automated fashion, we find that in most cases it's typically more useful to define Regions of Interest or ROI's to be saved for each pixel within a single data file. Each ROI defines the net counts in a given number of channels for a given fluorescence peak of interest, for example Fe Kα or Pb Lα1.

Data Processing and Compositional Calculations

Most of the XAFS or XRD data obtained at X26A can be evaluated using the same types of data processing techniques that most synchrotron users are aware of. Due to space limitations I won't go into detail on these here, since we've tried to make the data formats more or less standard. I will make two recommendations, however. For XAFS data we increasingly find that users are migrating towards the use of Thorsten Ressler's WinXAS program. It continues to be an impressive piece of software for XAFS analysis and we highly recommend it. Information can be found here:http://www.winxas.de/

For XRD analysis, our data are collected in Bruker's (what used to be Siemens) proprietary format. Luckily, an excellent freeware routine written by Andy Hamersley will read Bruker images and allow for calibration, integration, etc. Again, we highly recommended it and you can find information on this program here:
http://biocat1.iit.edu/fit2d/

With that out of the way I do want to spend some time discussing the calculation of elemental concentrations from the X26A energy dispersive data. As with instruments like the electron microprobe, ideally to calculate the concentration of an element from an XRF energy or wavelength dispersive spectra corrections must be made to account for differences in the absorption and fluorescence characteristics of samples and absorbers on the instrument (so called ZAF corrections in EMP analysis). On an electron microprobe this is somewhat simplified by the small interaction volume of the electron beam, generally restricting fluorescence to the surface of the sample. The X26A x-ray beam, however, is highly energetic and deeply penetrating, so that the escape depth of characteristic x-rays generated from the sample interaction with the incident x-ray beam is strongly affected by the density and atomic number of the material being analyzed. Additionally, since the analyses are done in air, the length (absorbance) of the air path between the sample and detector also affects these

calculations as a function of x-ray photon energy, less energetic x-rays being more strongly absorbed.

Therefore, two approaches are typically used, a standard based technique and one based on standard-less analysis. In the former, a standard containing the elements of interest in known concentrations is analyzed and used to determine the elemental sensitivities in terms of counts per unit beam flux. This can be a very accurate technique, particularly for low-density materials such as biological specimens where the overall average atomic number varies little and absorption is small. So, if your standard has all the elements that you're interested in relative to your unknown all you basically do is calculate concentration based on the relative fluorescent peak intensities of the unknown versus your standards. However, this technique assumes the standard and the unknown are identical with regards with density and thickness. In geological materials this is virtually never the case, but corrections for such effects can be made using the NRLXRF software (see below).

We find the latter approach typically more useful for geologic materials. In the standard-less approach we assume that the concentration of one of the detected elements in the "unknown" spectrum is known either by the results of another analytical technique, such as electron microprobe, or by stoichiometry (for example Ca abundance in calcite). In this case, the known element is used as a reference and the sensitivities relative to that element are computed theoretically for all other elements. We use a modified version of the public-domain software NRLXRF (from the Naval Research Laboratory; Criss, 1977). NRLXRF was written for conventional XRF analysis where one has a standard for every element of interest. Since trace element standards with micrometer scale homogeneity are rare, we have modified the program for "standard-less" analysis, i.e. theoretical estimation of elemental concentrations from an individual spectrum. Basically, a theoretical standard is created by normalization to a specific x-ray fluorescence line of known composition. Even in the standard-based analysis described above, corrections for matrix and thickness differences between the standard and the unknown must often be made but these corrections tend to be small when dealing with relative sensitivities. This program takes into account the absorption of the incident beam by Be windows, air, etc., photoionization efficiencies, fluorescence yields, self-absorption, secondary fluorescence, and fluorescence beam absorption by air and detector filters. As input parameters, NRLXRF needs:

- Either the synchrotron production spectrum calculated theoretically for white beam or the incident monochromatic beam energy
- The composition and thickness of incident beam filters
- Incident/take-off geometry
- Sample major element composition and thickness
- Composition and thickness of detector filters, including the detector to sample air path

Most of these parameters are fixed by beamline geometry and optics, and thus well known. The biggest challenge for the user is to determine the sample thickness in grams per unit area, which is crucial in accurately predicting self-absorption effects. Thickness can usually be estimated with sufficient accuracy on a high-powered, petrographic microscope by focusing on the top and bottom surfaces of a mineral grain, reading the differential height from the stage micrometer and correcting for the index of refraction. An estimate of the sample density is then also needed. With this information the concentrations can then be calculated in elemental weight percent.

For those interested in a more detailed explanation of our implementation of NRLXRF at X26A, we direct you to the following website:
http://cars9.uchicago.edu/sutton/snrlxrf_doc/snrlxrf.htm.

Applications and Examples

The microprobe can provide trace element compositions with 1-ppm detection sensitivity or better (SXRF), all elements (with Z> 16 or so) can be seen simultaneously, and it is usually easy to distinguish different elements.

Relative abundances of elements in particular can be quickly calculated with high precision and accuracy. For microXANES typically hundreds of ppm are required for relatively rapid characterization (although in practicality other factors such as the atomic number of the element of interest, average sample density, K vs. L shell absorption, etc. are factors as well). Numerous examples of the type of research conducted at X26A are available in PDF on our website at:
http://www.bnl.gov/x26a

X26A has long been used to provide information on redox chemistry and speciation (XANES) and constrain mineralogy and crystal chemistry (SXRD, EXAFS) at micron spatial resolutions. With these varying capabilities analyses can be directly coupled to petrographic, geochronologic, and EMPA data. The analyses can be done non-destructively and *in-situ*: analyses can be done on thin-sections, rock fragments, powders, soils, and biological materials, samples can be in solution, liquids,

amorphous solids, aggregates, plant roots, surfaces, etc. Trace element analyses can be performed on small (< 1 nanogram) specimens, particle analyses that are vital in atmospheric chemistry studies of transport and deposition of anthropogenic pollutants, natural atmospheric dust, and historical climatic reconstructions. Cometary and interplanetary particles smaller than 10 μm in diameter that are collected in the stratosphere can also be studied (see Flynn and Sutton's 1998 science highlight on the analysis of interplanetary dust particles at http://nslsweb.nsls.bnl.gov/nsls/pubs/actrpt/1998/2geo.pdf). Geochemical partitioning and migrational behavior can be studied at concentration levels found in nature without the need for sample preconcentration or pre-conditioning (see Tokunaga et al's 2001 science highlights on chromate diffusion in soils at http://nslsweb.nsls.bnl.gov/nsls/pubs/actrpt/2001/sec2_scihi_geo_tokunaga.pdf). Such information is crucial in inferring the physio-chemical evolution of earth and environmental systems. In biologic systems, trace metals can be studied with few beam effects on the sample and without the need for any special sample preparation (see Lanzirotti et al's 2001evaluation of methyl mercury in human hair tissue at http://nslsweb.nsls.bnl.gov/nsls/pubs/actrpt/2001/sec2_scihi_geo_lanzirotti.pdf). In agricultural and phytoremediation studies this means that plant materials can be analyzed without the need for drying the sample, which can affect metal distribution (for example see Ross et al's 2000 highlight on Pb association with Mn oxides in soils at http://www.pubs.bnl.gov/nsls00/pdf/2_scihi_env.pdf or Schulze et al's 1999 highlight on the effects of soil fungi on Mn reduction at http://www.pubs.bnl.gov/nsls99/pdf/2env.pdf). In toxicology studies trace metals such as Hg, Pb, Cr, Se, As can all be analyzed in tissue sections. Actinides can be studied in-situ to better understand their chemical behavior in rocks and soils, studies critical to evaluating remediation and storage of nuclear waste sites (for example see Duff et al's 1999 highlight on Pu sorption in Yucca Mountain rocks at http://www.pubs.bnl.gov/nsls99/pdf/2env.pdf or studies of U chemistry in ancient systems by McCall et al. at http://nslsweb.nsls.bnl.gov/nsls/pubs/actrpt/2001/sec2_scihi_geo_mccall.pdf and Lanzirotti et al. at http://www.pubs.bnl.gov/nsls00/pdf/2_scihi_geo_b.pdf A list of selected papers generated by the x-ray microprobe research is given below for further details on this work.

Recent X26A Publications

Astheimer, R., B. Kristin, G.E. Brown, Jr., J. Hoy, K.W. Jones, N.C. Sturchio, S.R. Sutton, G.A. Waychunas, N.B. Woodward (2000) Inside Rocks. Geotimes, American Geological Institute, 20-23.

Banas, A., Kwiatek, W.M., Zajac, W. (2001) Trace element analysis of tissue section by means of synchrotron radiation: the use of GNUPLOT for SRIXE spectra analysis. Journal of Alloys and Compounds, 328, 135-138.

Bassett, W.A., Anderson, A.J., Mayanovic, R. A., and Chou, I.-Ming (2000) Hydrothermal diamond anvil cell for XAFS studies of first-row transition elements in aqueous solution up to supercritical conditions Chemical Geology, 167, 3-10.

Becker, A., W. Klöck, K. Friese, P. Schreck, H.-C. Treutler, B. Spettel, M.C. Duff and W. Eisenächer (2001) Lake Süßer See as a Natural Sink for Heavy Metals from Copper Mining. J. Geochem. Exploration 74 (1-3): 205-217

Bender, J., M.C. Duff, P. Phillips and M. Hill (2000) Bioremediation and Bioreduction of U(VI) in Groundwaters by Microbial Mats. Environ. Sci. Technol 34(15), 3235-3241.

Bertsch, P.M., and D.B. Hunter (1998) Elucidating fundamental mechanisms in soil and environmental chemistry: The role of advanced analytical and spectroscopic methods. Soil Sci. Soc. America Special Publication 55, "Future Prospects for Soil Chemistry," 103-122.

Bloodaxe, E.S., Hughes, J.M., Dyar, M.D., Grew, E.S., and Guidotti, C.V. (1999) Tourmaline: Linking structure and chemistry. Am. Min., 84, 922-928.

Bosze, S., and J. Rakovan (1999) Surface Controlled Heterogeneous Incorporation of REE, Sr and Y in Fluorite. Annual Geological Society of America meeting, Abstracts with program. p. A-358, 1999.

Bosze, S., and J. Rakovan (2002) Surface Structure Controlled Sectoral Zoning of the Rare Earth Elements in Fluorite from Long Lake, N.Y. and Bingham, N.M. Geochim. Cosmochim. Acta, in press.

Chouparova, E., H. Feng, A. Lanzirotti, and K. Jones (2000) Trace metal distributions in rod wax deposits formed in an oil-producing well, Andarko Basin, Oklahoma," in Seventh Annual Internat. Petroleum Environmental Conference.

Cole, J.M., Nienstedt, J., Spataro, G., Rasbury, E.T, Lanzirotti, A., Celestian, A.J., Nilsson, M., Hanson, G.N. (2002) Phosphor imaging as a tool for in situ mapping of ppm levels of uranium and thorium in rocks and minerals. Chemical Geology (in press).

Dalpe, C. and D.R. Baker (2000) Experimental investigation of large-ion-lithophile-element-, high-field-strength-element- and rare-earth-element-partitioning between calcic

amphibole and basaltic melt: the effects of pressure and oxygen fugacity. Contrib. Mineral. Petrol. 140: 233-250.

Davenport, A. J., M.P. Ryan, M.C. Simmonds, P. Ernst, R. C. Newman, S.R. Sutton, and J.S. Colligon (2001) In situ synchrotron x-ray microprobe studies of passivation thresholds in Fe-Cr alloys. Jour. Electrochem. Soc., 148 (6): B217-B221.

Delaney, J. S., M.D. Dyar and S.R. Sutton (2001) Quantifying x-ray pleochroism effects in synchrotron micro-XANES microanalyses of elemental oxidation states: feldspar and biotite. Lunar. Planet. Sci. XXXII, 1936.

Delaney, J. S., M.D. Dyar, S. R. Sutton, and S. Bajt (1998) Redox ratios with relevant resolution: Solving an old problem using the synchrotron microXANES probe. Geology 26, 139-142.

Delaney, J.S., M.D. Dyar, and S.R. Sutton (2000) Correction of the calibration of ferric/ferrous determinations in pyroxene from Martian samples and achondritic meteorites by synchrotron microXANES spectroscopy. Lunar Planet. Sci. XXXI, 1981.

Delaney, J.S., S.R. Sutton, M. Newville, J.H. Jones, B. Hanson, M.D. Dyar and H. Schreiber (2000) Synchrotron micro-XANES measurements of vanadium oxidation state in glasses as a function of oxygen fugacity: Experimental calibration of data relevant to partition coefficient determination. Lunar Planet. Sci. XXXI, 1806.

Duff, M.C. (2000) Speciation and Transformations of Sorbed Pu on Geologic Materials: Wet Chemical and Spectroscopic Observations. In Plutonium in the Environment. In: Environmental Radioactivity Series 1, Elsevier Sci. Limited and Kyoto University, Osaka, Japan, 464 pp.

Duff, M.C., J.U. Coughlin and D.B. Hunter (2002) Uranium Co-precipitation with Fe Oxide Minerals. Geochim. Cosmochim. Acta (in press).

Duff, M.C., D.B. Hunter, I.R. Triay, P.M. Bertsch, D.T. Reed, S.R. Sutton, G. Shea-McCarthy, J. Kitten, P. Eng, S.J. Chipera and D.T. Vaniman (1999) Mineral Associations and Average Oxidation States of Sorbed Pu on Tuff. Environ. Sci. Technol. 33, 2163-2169.

Duff, M.C., D.B. Hunter, I.R. Triay, P.M. Bertsch, J. Kitten and D.T. Vaniman (2001) Comparison of Two Micro-Analytical Methods for Detecting the Spatial Distribution of Sorbed Pu on Geologic Materials. J. Contam. Hydrol. 47. 211-218

Duff, M.C., D.B. Hunter, P.M. Bertsch and C. Amrhein (1999) Factors Influencing Uranium Reduction and Solubility in Evaporation Pond Sediments. Biogeochemistry 45, 95-114.

Duff, M.C., D.E. Morris, D.B. Hunter and P.M. Bertsch (2000) Spectroscopic Characterization of Uranium in Evaporation Basin Sediments. Geochim. Cosmochim. Acta 46, 1535-1550.

Duff, M.C., M. Newville, D.B. Hunter, P.M. Bertsch, S.R. Sutton, I.R. Triay, D.T. Vaniman, P. Eng and M.L. Rivers (1999) Micro-XAS Studies with Sorbed Plutonium on Tuff. J. Synchrotron Radiation 6, 350-352.

Durda, D.D., and G.J. Flynn (1999) Experimental Study of the Impact Disruption of a Porous, Inhomogeneous Target. Icarus 142, 46-55.

Dyar, M. D., D.E. Polyak, J.S. Delaney, S.R. Sutton, S.A. McEnroe, and C. Tegner, (1999) Feldspar with and without micro-inclusions: Ferric iron determination by SmX. Geological Society of America, Annual Meeting, Denver, A-358.

Dyar, M.D., J. Delaney, S.R. Sutton and M. Schaefer (1998) Fe^{3+} distribution in oxidized olivine: A synchrotron micro-XANES study. Am. Mineral. 83, 1361-1365.

Dyar, M.D., J.S. Delaney, and S.R. Sutton (2001) Fe XANES spectra of iron-rich micas. Eur. Jour. Min., Mica Special Issue, 13 (6): 1079-1098.

Dyar, M.D., J.S. Delaney, P.D. Kinny, and C.M. Graham, C.M. (2000) Implications of dehydrogenation processes in amphibole for planetary hydrogen and oxygen budgets. Lunar Planet. Sci. XXXI, 1768.

Dyar, M.D., M. Wiedenbeck, L. Cross, J.S. Delaney, C.A. Francis, E.S. Grew, C.V. Guidotti, R.L. Hervig, J.M. Hughes, W. Leeman, A.V. McGuire, R.L. Paul, J.D. Robertson, and M. Yates (2000) Mineral standards for microanalysis of light elements. Geoanalysis 2000, Pont à Mousson, Lorraine France.

Dyar, M.D., Delaney, J.S., Rossman, G.R., and Sutton, S.R. (2002) Polarized XANES spectra of feldspar: Calibration and interpretation. Amer. Mineral., submitted.

Dyar, M.D., Gunter, M.E., Delaney, J.S., Lanzarotti, A., and Sutton, S.R. (2002) Systematics in the structure, optical properties, and XANES spectra of pyroxenes, amphiboles, and micas. Canad. Mineral., submitted.

Dyar, M.D., J.S. Delaney and S.R. Sutton (2000) Advances in interpretation of Fe XANES pre-edge spectra and resultant improvements in microanalysis of ferric/ferrous ratios on thin sections. Lunar Planet. Sci. XXXI, 1337.

Eng, P.J., Rivers, M., Yang, B.X., and Schildkamp, W. (1995). Micro-focusing 4keV to 65keVx-rays with bent Kirkpatrick-Baez mirrors. X-ray microbeam technology and applications, Proc. SPIE 2516, 41-51.

Flynn, G.J., and S.R. Sutton (1998) Trace element contents of L2011 cluster fragments: Implications for comet Schwassman-Wachmann-3 as the source of L2011 cluster particles. Meteoritics 33, A49-A50.

Flynn, G.J., D. Alger, A. Lanzirotti and S.R. Sutton (2000) Combined x-ray diffraction mineralogical classification and x-ray fluorescence chemical analysis of individual interplanetary dust particles. Lunar Planet. Sci. XXXI, 1772.

Flynn, G.J., S.R. Sutton and F. Horz (2000) Synchrotron x-ray microprobe in-situ analyses of extraterrestrial particles collected in aerogel on the Mir space station. Lunar Planet. Sci. XXXI, 1457.

Flynn, G.J., S.R. Sutton, K. Kehm, and C.M. Hohenberg (1998) Volatile components of large and small IDPs from L2036: Comparison of Zn and He heating indicators. Meteoritics 33, A51.

Flynn, G.J., S.R. Sutton, and A. Lanzirotti (2000) A Comparison of the Selenium Contents of Sulfides from Interplanetary Dust Particles and Meteorites. Meteoritics and Planetary Science 35, A54.

Fredrickson, J.K., J.M. Zachara, D.W. Kennedy, M.C. Duff, Y.A. Gorby, S.W. Li and K.M. Krupka (2000) Reduction of U(VI) in Goethite (?-FeOOH) Suspensions by a Dissimilatory Metal-Reducing Bacterium. Geochim. Cosmochim. Acta 64, 3085-3098.

Fredrickson, J.K., J.M. Zachara, D.W. Kennedy, C. Li, M.C. Duff, D.B. Hunter and A. Dohnalkova (2002) Influence of Mn Oxides on the Bioreduction of U(VI) by the Metal-Reducing Bacterium *Shewanella putrefaciens*. Geochim. Cosmochim. Acta (in press).

Fuhrmann, M., S. Bajt and M. Schoonen (1998) Sorption processes on iodine on minerals. Applied Geochemistry 13, 127-141.

Halada, G.P., C.R. Clayton, M.J. Vasquez, J.R. Kearns, M.W. Kendig, S.L. Jeanjaquet, G.G. Peterson and G. Shea-McCarthy (1998) Spatially Resolved Microchemical Analysis of Chromate Conversion Coated Aluminum Alloys and Constituent Intermetallic Particles. In Critical Factors in Localized Corrosion III —Jerome Kruger 70th Birthday Symposium, The Electrochemical Society.

Herzog, G.F., G. J. Flynn, S. R. Sutton, J.S. Delaney, A. N. Krot, and A. Meibom (2000) Low Gallium and Germanium Contents in Metal grains from the Bencubbib-Like Meteorite Queen Alexndr Range 94411 Determined by Synchrotron X-Ray Fluorescence Analysis. Meteoritics and Planetary Science 35, A71.

Hunter, D.B. and P.M. Bertsch (1998) In Situ Examination of Uranium Contaminated Soil Particles by Micro-X-Ray Absorption and Micro-Fluorescence Spectroscopies. Journal of Radioanalytical and Nuclear Chemistry 234, 237-242.

Hunter, D.B., W.P. Gates, P.M. Bertsch and K.M. Kemner (1999) Degradation of Tetraphenylboron at Hydrated Smectite Surfaces Studied by Time Resolved IR and X-Ray Absorption. Mineral Water Interfacial Reactions: Kinetics and Mechanisms. Eds. D.L. Sparks and T.J. Grundl. American Chemical Society Symposium Series, Volume 715, Chapter 14, 282-300.

Isaacs, H.S., C.S. Jeffcoate, A.J. Aldykiewicz, M.P. Ryan, M. Kaneko, G. Shea-McCarthy (2000) Scanning Volta Potentials and Polarization Measurements of Metals in Irradiated Air. Electrochem. Solid-State Letters 3, 253-255.

Jones, K.W. (1999) Application of Synchrotron Radiation in the Geological and Environmental Sciences. In K.Janssens, A.Rindby, and F.Adams, Microscopic X-ray Fluorescence Analysis, J. Wiley & Sons, Sussex, 434 pp.

Jones, K.W., and H. Feng (2000) Microanalysis of materials using synchrotron radiation. In T.K.Sham, ed., Chemical Applications of Synchrotron Radiation, World Sci Pub., NJ.

Kehm, K., G.J. Flynn, C.M. Hohenberg, R.L. Palma, R.O. Pepin, D. J. Schlutter, S.R. Sutton, and R.M. Walker (1999) A consortium investigation of possible cometary IDPs. Lunar Planet. Sci. XXX, 1398.

Kehm, K., G.J. Flynn, S.R. Sutton, and C.M. Hohenberg (1998) Combined noble gas and trace element measurements on single idps from the L2036 collector. Lunar Planet. Sci. XXIX, 1970.

King, P.L., R.L. Hervig, J.R. Holloway, J.S. Delaney, and M.D. Dyar (2000) Partitioning of Fe^{3+}/Fe total between amphibole and basanitic melt as a function of oxygen fugacity. Earth Planet. Sci. Lett. 178, 97-112.

Kwiatek, W.M., Galka, M., Hanson, A.L., Paluszkiewicz, C., and Cichocki, T. (2001) XANES as a tool for iron oxidation state determination in tissues Journal of Alloys and Compounds, 328, 276-282.

Kwiatek, W.M., Kubica, B., Paluszkiewicz, C., Galka, M. (2001) Trace element analysis by means of synchrotron radiation, XRF, and PIXE: selection of sample preparation procedure. Journal of Alloys and Compounds, 328, 283-288.

Lanzirotti, A., M. Becker, G.N. Hanson and S. Sutton (2001) Combined synchrotron microbeam x-ray fluorescence, XANES and diffraction analysis of uranium enriched phosphates. Eos Trans. AGU 82(20), S414.

Mancini, F., Alviola, R., Marshall, B., Fujimoto, K., Papunen, H., Dyar, M.D., and Delaney, J.S. (2002) Pyroxferroite from Vittinki, SW Finland: crystal structure, chemistry, and petrologic implications. Canad. Mineral., in press.

Mann, S. E., M.C. Ringo, G. Shea-McCarthy, J.E. Penner-Hahn, and C.E. Evans (2000) Element-Specific Detection in Capillary Electrophoresis using X-ray Fluroescence Spectroscopy. Anal. Chem. 72, 1754-1758.

Marques, J. J. (2000) Trace Element Distributions in Brazilian Cerrado Soils at the Landscape and Micrometer Scales. Ph.D. Dissertation, Purdue University.

Marques, J. J., D.G. Schulze, N. Curi, and S.A. Mertzman (2000) Trace Elements in Oxisols from the Brazilian Cerrado: I. Landscape Scale Relationships," Soil Science Society of America annual meeting.

Martin, R.R., T.K.Sham, K.W. Jones, and R. Protz (1998) Secondary ion mass spectrometry and synchrotron x-ray fluorescence in the study of the variation in metal content with time in tree rings. Canadian Journ. Of Forest Res. 28, 1464-1470.

Martin, R.R.; Sham, T.K.; Won, G.W.; Jones, K.W.; Feng, H. (2001) Synchrotron X-ray fluorescence and secondary ion mass spectrometry in tree ring microanalysis: applications to dendroanalysis. X-ray Spectrometry, 30, 338-341.

Mosbah, M., Duraud, J.P., Métrich, N., Wu, Z., Delaney, J.S., San Miguel, A. (1999) Micro-XANES with synchrotron radiation: a complementary tool of micro-PIXE and micro-SXRF for the determination of oxidation state of elements. Application to geological materials Nuclear Instruments and Methods in Physics Research Section B: Beam Interactions with Materials and Atoms, 158, 214-220

Naftel, S., Martin, R., Sham, T., Macfie, S., and Jones, K. (2001) Micro-synchrotron x-ray fluorescence of cadmium-challanged corn roots. J. Electron. Spectrosc. Relat. Phenom. 119, 235-239.

Paluszkiewicz, C., and Kwiatek, W. (2001) Analysis of human cancer prostate tissue using FTIR microspectroscopy and SRIXE techniques. J. Mol. Struct., 565-566, 329-334.

Reeder, R.J., and J. Rakovan (1999) Surface structural controls on trace element incorporation during crystal growth. In Growth, Dissolution and Pattern-formation in Geosystems, B. Jamtveitand P. Meakin (eds.), 143-162. Kluwer Academic Publishers.

Reeder, R.J., Nugent, M., Tait, C.D., Morris, D.E., Heald, S.M., Beck, K.M., Hess, W.P. and Lanzirotti, A. (2001) Coprecipitation of Uranium(VI) with Calcite: XAFS, Micro-XAS, and Luminescence Characterization. Geochimica et Cosmochimica Acta 65, 3491-3503.

Righter, K., M.D. Dyar, J.S. Delaney, T.W. Vennemann, and R.L. Hervig (2002) Distribution of OH, O, CL, and F in biotite from volcanic rocks and correlations with octahedral cations. Amer. Mineral., 87 (1): 142-153.

Ringo, M.C., M.S. Huhta, G. Shea-McCarthy, J.E. Penner-Hahn, C.E. Evans (1999) On-Line X-ray Fluorescence Detection for Capillary Electrophoresis Separations. Nucl. Instr. Meth. B 149, 177-181.

Roberts, D.R., A. Scheinost and D.L. Sparks (2002) Zinc speciation in smelter-contaminated soils in the vicinity of the historic Palmerton smelter: A multi-analytical approach. Environ. Sci. Technol., in press.

Ross, D. S., H.C. Hales, and A. Lanzirotti (2001) Sensitivity of soil Mn-oxides: XANES spectroscopy of moist soils causes reduction. Soil Sci. Soc. Amer. J. 65, 744-752.

Ross, D. S., H.C. Hales, and A. Lanzirotti (2001) Sensitivity of soil Mn-oxides: drying and storage causes reduction. Soil Sci. Soc. Of Amer. J. 65, 736-743.

Schnabel, C., G. F. Herzog, J. S. Delaney, S. R. Sutton, and G. J. Flynn (1998) Microdistribution of Zn in chondrites. Lunar Planet. Sci. XXIX, 1738.

Sham, T. K., R.R. Martin, K.W. Jones, R. Protz, W. Skinner, and B. Hale (1999) Secondary ion mass spectrometry and synchrotron x-ray fluorescence in dendroanalysis: molecular environmental science. In 8th European conference on applications of surface and interface analysis.

Steele, I.M; Cabri, L.J.; Gaspar, J.; McMahon, G.; Marquez, M.A., Vascocellos, A.A.Z. (2000) Comparative analysis of sulfides for gold using SXRF and SIMS. Canadian Mineralogist, 38, 1-10.

Sturchio, N. C., M. R. Antonio, L. Soderholm, S. R. Sutton, and J. C. Brannon (1998) Tetravalent uranium in calcite. Science 281, 971-973.

Sutton, S. R, G. J. Flynn, M. Rivers, P. Eng, and M. Newville (1999) Trace element analyses of L2011 cluster particles with the new x-ray microprobe at the Advanced Photon Source. Lunar Planet. Sci. XXX, 1656.

Sutton, S.R., and M.L. Rivers (1999) Hard x-ray synchrotron microprobe techniques and applications. In CMS Workshop Lectures, Vol. 9, Synchrotron Methods in Clay Science, D. G. Schulze, Stucki, J. W., and Bertsch, P. M. eds., 146-163, The Clay Minerals Society, Boulder, CO.

Sutton, S.R., G.J. Flynn, M. Rivers, P. Eng, M. Newville, G. Shea-McCarthy, and A. Lanzirotti (1999) Trace Element Chemical Analysis with Synchrotron-Based X-Ray Microprobes. Meteoritics & Planet. Sci. 34, A113-114.

Sutton, S. R., M.L. Rivers, P. J. Eng and M. Newville (1999) Applications of synchrotron x-ray microprobe analysis in geochemistry and cosmochemistry. Eos Trans. AGU 78, F789.

Tokunaga, T. K., J. Wan, and S.R. Sutton (2000) Transient film flow on rough fracture surfaces. Water Resources Research 36, 1737-1746.

Tokunaga, T. K., J. Wan, M. K. Firestone, T. C. Hazen, K. R. Olson, D. Herman, S. R. Sutton, and A. Lanzirotti (2002) In-situ Reduction of Cr(VI) in Contaminated Soils Through Organic Carbon Amendment. In preparation.

Tokunaga, T., S. R. Sutton, S. Bajt and P. Nuessle (1998) Selenium diffusion and reduction at the water-sediment boundary: Micro-XANES spectroscopy of reactive transport. Environ. Sci. Tech.32, 1092-1098.

Vaniman, D.T., S.J. Chipera, D.L. Bish, M.C. Duff and D.B. Hunter (2002) Crystal Chemistry of Clay - Mn Oxide Associations in Soils, Fractures, and Matrix of the Bandelier Tuff, Pajarito Mesa, New Mexico. Geochimica et Cosmochimica Acta (in press).

Vanko, D.A., M. Bonnin-Mosbah, P. Philippot, E. Rodder and S.R. Sutton (2001) Fluid Inclusions in Quartz from Oceanic Hydrothermal Specimens and the Bingham, Utah, Porphyry-Cu Deposit: A Study with PIXE and SXRF, Chemical Geology, (173) 1-3, 227-238.

Walker, S.R., H.E. Jamieson, S.R. Sutton, and A. Lanzirotti (2002) Arsenic oxidation state heterogeneity and correlations with mineralogy in mine waste solids from Yellowknife. Geological Association of Canada, Saskatoon, submitted.

Wu, Z., Bonnin-Mosbah, M., Duraud, J., Metrich, N., and Delaney, J. (1999) XANES studies of Fe-bearing glasses. J. Synch. Rad., 6, 344-346.

Xirouchakis, D., Draper, D.S., Schwandt, C.S., and Lanzirotti, A. (2002) Crystallization conditions of Los Angeles, a basaltic Martian meteorite. Geochimica et Cosmochimica Acta , 66, 1861-1874.

Yun, W., S.T. Pratt, R.M. Miller, Z. Chai, D.B. Hunter, A.G. Jarstfer, K.M. Kemner, B. Lai, H.-R. Lee, D.G. Legnini, W. Rodriguez, and C.I. Smith (1998) Hard X-Ray Imaging and Microspectroscopy of micorrhizal symbionts. J. Synchrotron Research. 5, 1390-1395.

Acknowledgements

We'd like to acknowledge the dedicated moral and economic support of our PRT representatives, in particular Steve Sutton and Mark Rivers for CARS, Paul Bertsch for SREL, and Keith Jones for BNL-Env.Sci. Much of this article is based on a workshop article written for a 1992 NSLS workshop organized by our former beamline local contact Sasa Bajt. We'd also like to acknowledge our beamline staff, both current (Bill Rao) and former (Grace Shea-McCarthy and Pat Nuessle). Lastly, we thank DOE's Geosciences Research Program for their continued economic support of the X26A beamline and the NSLS for maintaining the high level of commitment to the quality of the facility.